analytical chemistry

pubs.acs.org/ac Article

An Electrochemical Biosensor Designed by Using Zr-Based Metal–Organic Frameworks for the Detection of Glioblastoma-Derived Exosomes with Practical Application

Zhaowei Sun, Lei Wang, Shuai Wu, Yanhong Pan, Yu Dong, Sha Zhu, Jie Yang, Yongmei Yin,* and Genxi Li*

Cite This: *Anal. Chem.* 2020, 92, 3819–3826 Read Online

ACCESS | Metrics & More | Article Recommendations | Supporting Information

ABSTRACT: Glioblastoma (GBM) is one of the most fatal tumors in the brain, and its early diagnosis remains technically challenging due to the complex repertoires of oncogenic alterations and blood-brain barrier (BBB). GBM-derived specific exosomes can cross the BBB and circulate in body fluids, so they can be noninvasive biomarkers for the early diagnosis of GBM. Herein, we propose a sensitive and label-free electrochemical biosensor designed by using Zr-based metal–organic frameworks (Zr-MOFs) for the detection of GBM-derived exosomes with practical application. In the design, a peptide ligand can specifically bind with human epidermal growth factor receptor (EGFR) and EGFR variant (v) III mutation (EGFRvIII), which are overexpressed on the GBM-derived exosomes. Meanwhile, Zr-MOFs encapsulated with methylene blue can absorb on the surface of the exosomes due to the interaction between Zr^{4+} and the intrinsic phosphate groups outside of exosomes. Consequently, the concentration of exosomes can be directly quantified by monitoring the electroactive molecules inside MOFs, ranging from 9.5×10^3 to 1.9×10^7 particles/μL with the detection of limit of 7.83×10^3 particles/μL. Furthermore, this proposed biosensor can distinguish GBM patients from healthy groups, demonstrating the great prospect for early clinical diagnosis.

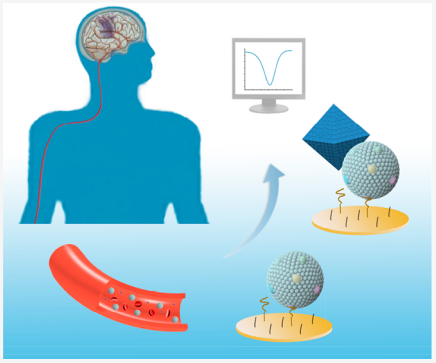

Glioblastoma (GBM) is known to be one of the most common and fatal malignant intracranial tumors in the brain, with widespread invasiveness, rapid cell proliferation, extensive angiogenesis, and poor prognosis.[1−3] The median survival of GBM patients remains 15−18 months, with the recurrence rate of 7 months, although the maximum treatment efforts including aggressive surgical resection and conventional therapy have been performed.[4−6] This dismal outcome is partly due to delayed diagnosis, thus early diagnosis of GBM plays an important role in improving the extremely poor prognosis and survival.[7,8] Currently, the general techniques such as magnetic resonance imaging (MRI) and computed tomography (CT) are employed for the diagnosis and prognosis of GBM.[9−11] However, those techniques are uneconomical; require sophisticated equipment and professional technicians, restricting the universal application in the early detection. Until now, no significant improvements have been achieved, since GBM contains various oncogenic alterations and it has blood-brain barrier (BBB), limiting the communications between brain cells and others.[8,12]

Exosomes are 40−150 nm extracellular vesicles released from cells and widely circulated in body fluids, such as blood, urine, and cerebrospinal fluid.[13,14] These membrane-enclosed vesicles containing abundant bioactive molecules can cross the BBB and mediate intercellular communication.[15−17] Growing evidence has revealed that the GBM-derived specific exosomes have great potential as noninvasive candidates for early diagnosis of GBM.[18−20] Noteworthy, exosomes from the GBM cells are characterized by highly expressed human epidermal growth factor receptor (EGFR), and the most common variant (v) III mutation (EGFRvIII).[21,22] Overexpression and mutation of EGFR as biomarkers occur in virtually all of the classical subtype GBMs, and the expression of EGFRvIII is correlated with its poor prognosis.[23,24] Thus, analysis of exosomes characterized with both EGFR and EGFRvIII will be advantageous in early diagnosis and pre- and postsurgical of GBM.[25] Nevertheless, conventional quantitative methods for exosomes detection, such as enzyme-linked immunosorbent assay (ELISA) and flow cytometry, require complicated sample pretreatment and specialized analytical instruments.[26−28] Although some new methods, particularly by using electrochemical technique, have been proposed with more convenience and sensitivity,[29−32] they have some limitations, for instance, uneconomical, and lack of specificity

Received: November 18, 2019
Accepted: February 6, 2020
Published: February 6, 2020

https://dx.doi.org/10.1021/acs.analchem.9b05241
Anal. Chem. 2020, 92, 3819−3826

Scheme 1. Schematic Diagram of (A) the Fabrication Process of MB@UiO-66-Based Nanoprobe and (B) the Principle of the Electrochemical Biosensor for the Detection of GBM-Derived Exosomes

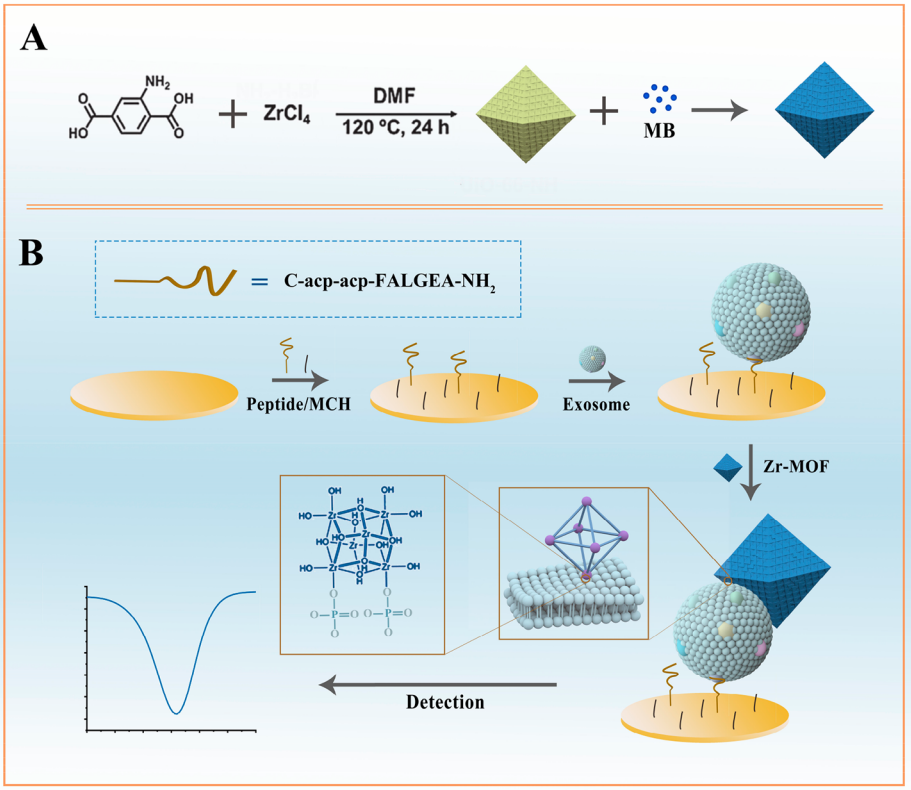

by using antibodies to detect common transmembrane proteins (e.g., CD 63, CD 9).[33,34] Therefore, it is very thrilling to design a novel method for detecting GBMs-derived exosomes rapidly, simply, and specifically.

Recently, metal−organic frameworks (MOFs) have emerged as a type of new material and widely explored for sensor design owing to their high surface areas, flexible porosity, chemical tenability, and durable sensing features.[35−38] The high porosity of MOFs offers an ability to accommodate a large number of electroactive molecules, and enhances their conductivity and analysis sensibility.[39,40] Particularly, Zr-MOFs have a high affinity to phosphate groups and have been used to selectively enrich phosphates biomolecules via the formation of Zr−O−P bonds.[41−44] As we know, exosomes are composed of phospholipid bilayers whose outer surface is surrounded with hydrophilic phosphate head. Inspired by these, we have proposed a label-free and enzyme-free electrochemical biosensor in this work for the analysis of GBM-derived exosomes relied on the interaction between the Zr−O clusters and intrinsic phospholipid bilayer of exosomes. In the design, a peptide ligand is modified on Au electrode that can specifically capture GBMs exosomes by selectively binding to EGFR and EGFRvIII.[25,45] Then, Zr-MOFs loaded with large numbers of electroactive methylene blue molecules (MB@UiO-66) approach to the electrode surface to generate a high electrochemical signal based on the combination between Zr^{4+} and the exosomes surface. Therefore, the concentration of exosomes can be directly quantified by monitoring the electrochemical signal inside Zr-MOF without extra recognition and amplification elements. Further study has shown that this method can distinguish GBM patients from healthy groups, and provide a simple, rapid, and universal platform for the early diagnosis of GBMs patients.

EXPERIMENTAL SECTION

Synthesis of UiO-66-NH_2 and MB@UiO-66. UiO-66-NH_2 was prepared according to our reported method.[38] For MB@UiO-66 preparation, 1 mg of MB mixed with 10 mg UiO-66-NH_2, and stirred in ultrapure water for 24 h at room temperature. The generated MB@UiO-66 precipitate was collected by centrifugation and washed with deionized water.

Elecrtode Treatment. The bare gold electrode was treated according to our pervious works.[46] First, the gold electrode was cleaned with piranha solution (sulfuric acid: H_2O_2 = 7:3) for 5 min followed by rinsing with ultrapure water. Then, the electrode was polished with alumina slurry (1 μm, 0.3 μm, and 0.05 μm) and sonicated in ethanol and distilled water for 5 min, respectively. Finally, the electrode was soaked in nitric acid (50%) for 30 min, and electrochemically cleaned in 0.5 M H_2SO_4 by scanning the potential between the oxidation and reduction of gold (−0.35 and 1.5 V). The modified electrodes were then rinsed with double-distilled water and dried with nitrogen.

Detection of Exosomes. The prepared gold electrode was incubated with 5 μM designed peptide containing 5 mM TCEP for 16 h at 4 °C, followed by blocking with 1 mM MCH solution at room temperature for 2 h. TCEP was used as a reducing agent to prevent the formation of disulfide bond of cysteine terminal.[47] MCH is used to block the blank sites of electrode surface and replace the nonspecific adsorption.[48] After rinsing with ultrapure water and drying with nitrogen, the electrodes were interacted with different concentrations (10 μL) exosomes in Tris-HCl (50 mM Tris and 150 mM NaCl,

https://dx.doi.org/10.1021/acs.analchem.9b05241
Anal. Chem. 2020, 92, 3819−3826

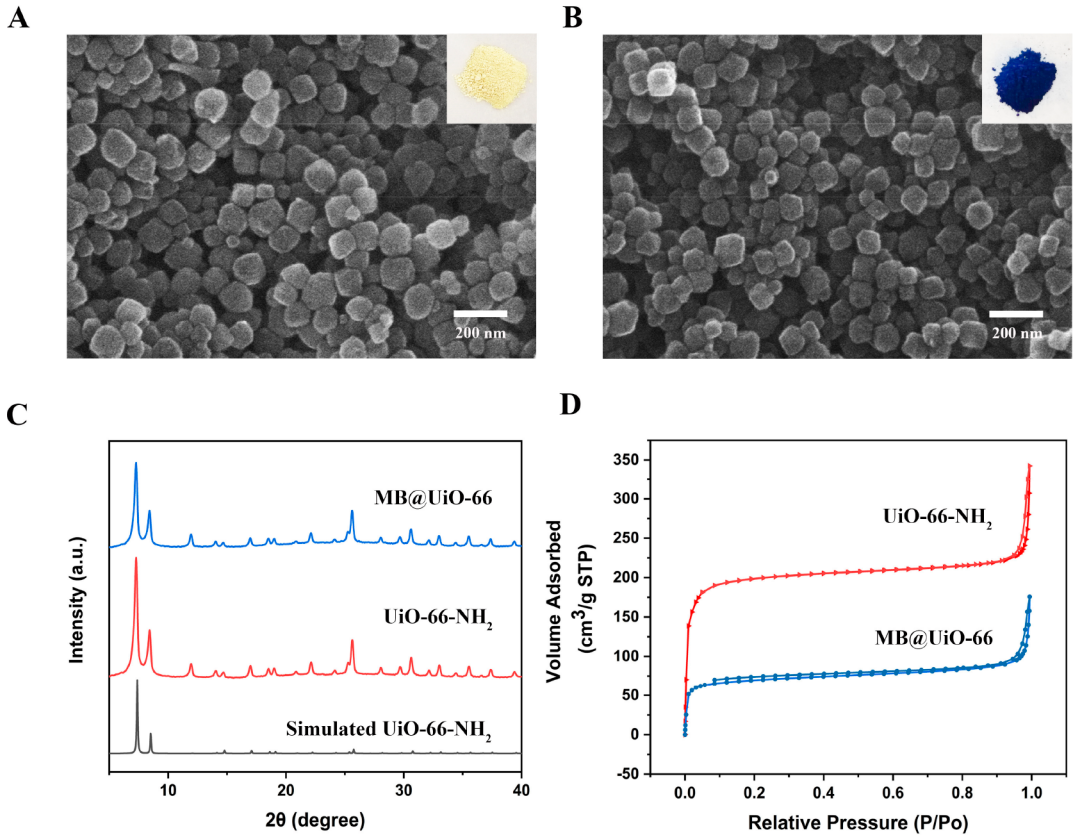

Figure 1. (A) SEM images of the UiO-66-NH_2 and (B) MB@UiO-66 (insets are the photographs). (C) Powder XRD patterns of simulated UiO-66-NH_2, as-synthesized UiO-66-NH_2, and MB@UiO-66. (D) Nitrogen adsorption−desorption isotherm of UiO-66-NH_2 and MB@UiO-66.

PH 7.4) for 2 h at room temperature. Afterward, the electrode was rinsed and dipped in 5% Tween-20 for 20 min to exclude unspecific adsorption. Then, 5 μL of the prepared MB@ Zr-MOF solution was dropped on the electrode surface and incubated for 30 min at room temperature. Finally, the modified electrode was thoroughly washed for electrochemical measurements.

Electrochemical Measurements. Electrochemical measurements were carried out on a CHI660D Potentiostat (CH Instruments) with a conventional three-electrode system. The gold electrode modified with peptides as the working electrode, a saturated calomel electrode (SCE) as the reference electrode, and a platinum wire as the counter electrode. The electrochemical impedance spectra (EIS) measurements was recorded in 5 mM $[Fe(CN)_6]^{3-/4-}$ electrolyte containing 1 M KCl, and the detailed experimental parameters were as follows: bias potential, 0.175 V; frequency range, 0.1−10 kHz; amplitude, 5 mV. Square wave voltammograms (SWVs) was scanned from −0.4 to −0.1 V in Tris-HCl solution and the detailed experimental parameters were as follows: step potential, 4 mV; frequency, 15 Hz; amplitude, 25 mV.

Other experimental details are described in Supporting Information (SI).

RESULTS AND DISCUSSION

The Principle of the Biosensor. In this study, a label-free electrochemical biosensor for the detection of GBM derived exosomes has been proposed and the principle of the design is depicted in Scheme 1. First, UiO-66-NH_2, a typical Zr-MOF, is chosen and synthesized through a reported method with slight modification.[38] Then, the MB@UiO-66-based nanoprobe is generated by stirring MB and UiO-66-NH_2 at room temperature. As well-known, MB is an electroactive redox indicator which is widely used to produce electrochemical signals on the electrode surface.[49,50] The high porosity of MOFs can load large numbers of MB, thus resulting in a high signal and improving the sensitivity of the biosensor. In the meantime, a designed peptide (H−C-acp-acp-FALGEA-NH_2) containing a protein binding motif is assembled as the sensing layer on the electrode surface by formation of Au−S bond through the cysteine and gold electrode.[25,45] The peptide is elongated at N-terminal with 6-aminocaproic acid to increase its flexibility, and amination is designed at C-terminal to reduce the electrostatic adsorption. Consequently, the peptide can selectively recognize EGFR/EGFRvIII and capture GBM-derived exosomes through the specific molecular recognition. After that, the functional MB@Zr-MOFs will combine with GBM-derived exosomes and produce a highly amplified electrochemical signal by the interaction between Zr^{4+} and the phosphate head of exosomes. As a result, the biosensor can be employed for the quantitative analysis of exosomes, sensitively, quickly, and simply.

Characterization of MOFs. The morphology and structure of UiO-66-NH_2 is characterized by scanning electron microscope (SEM) and X-ray diffraction (XRD). As illustrated in Figure 1A,C, the size of MOF is about 100 nm with uniform shape, and the sharp diffraction peaks of XRD are consistent with the simulated, which reveal the successful synthesis of the MOF. After electrochemical dyes are loaded into UiO-66-NH_2, the SEM results are basically the same except for the color change (Figure 1B). The XRD data preserve all diffraction peaks, suggesting that loading of dyes makes little influence on

https://dx.doi.org/10.1021/acs.analchem.9b05241
Anal. Chem. 2020, 92, 3819−3826

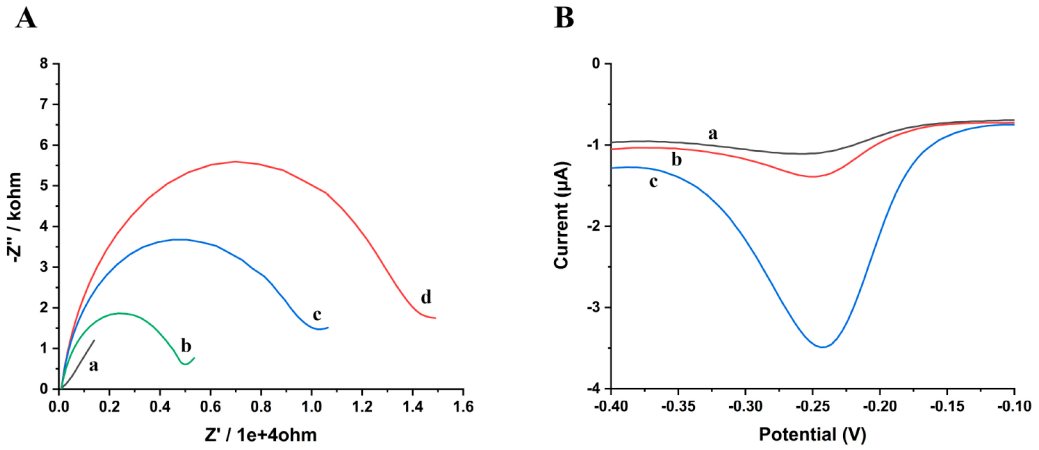

Figure 2. (A) EIS corresponding to the stepwise treatment of the electrode. Curves (a−d) represent separately the cases of the bare gold electrode, the electrode after modification with peptide, incubation with the exosomes, and labeled with MB@UiO-66. (B) SWV responses obtained on the cases with bare electrode (a), exosomes-free (b), and 1.9×10^7 particles/μL exosomes.

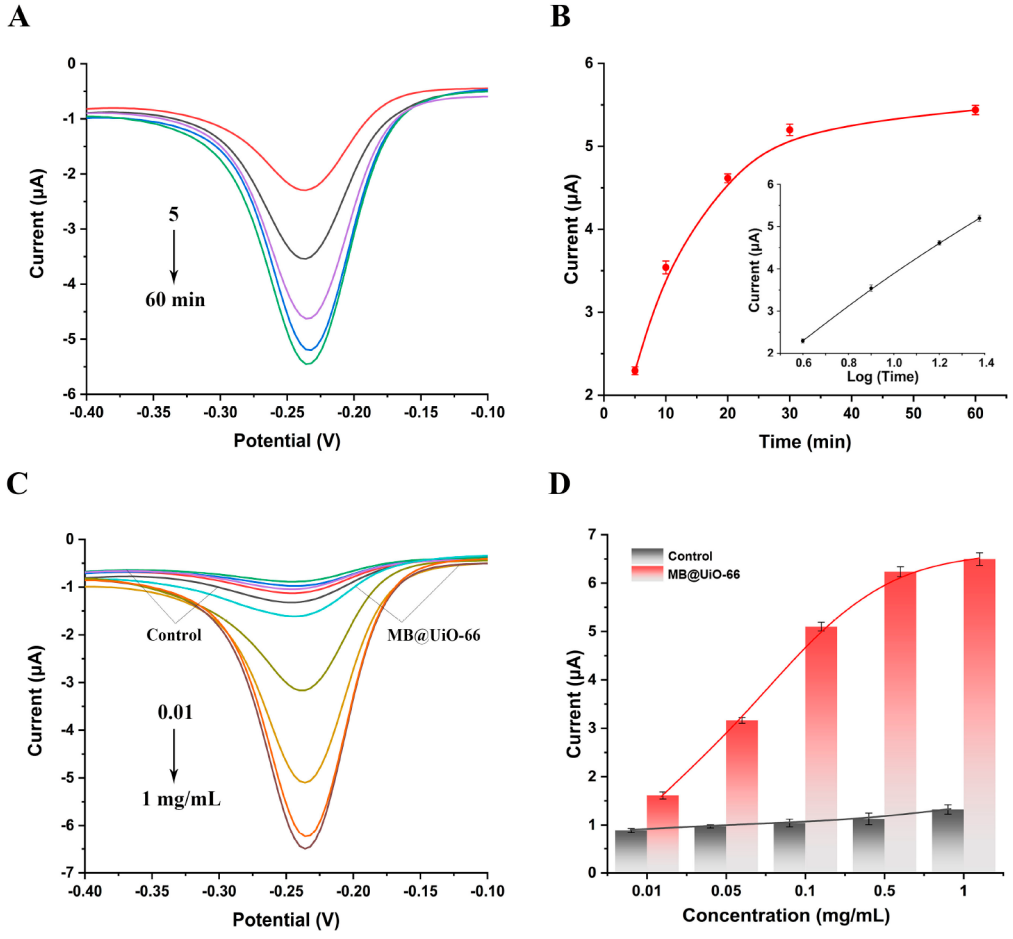

Figure 3. (A) SWV recorded with different incubation time of MB@UiO-66. (B) Relationship between the values of peak current and the incubation time. Inset is the linear range. Error bars represent the standard derivation of three independent experiments. (C) SWV recorded with different concentrations of MB@UiO-66. (D) Relationship between the values of peak current and the concentrations. Error bars represent the standard derivation of three independent experiments.

the crystalline structure. In order to further verify the successful fabrication of the nanoprobe, adsorption−desorption isotherm is performed at 77 K (Figure 1D). It can be calculated that the Brunauer−Emmett−Teller surface area of UiO-66 is 643 m^2/g, whereas the MB@UiO-66 is 227 m^2/g, which confirms that MBs are effectively encapsulated. In addition, Fourier transform infrared spectroscopy (FT-IR) has been conducted to investigate the variation (SI Figure S1). The characteristic peak at 1593 cm^{-1} originating from the vibrations of C═C in the benzene ring is enhanced, indicating the increase of the aromatic compounds. Besides, new characteristic peaks at 1343 cm^{-1}, 948 cm^{-1}, and 886 cm^{-1}

https://dx.doi.org/10.1021/acs.analchem.9b05241
Anal. Chem. 2020, 92, 3819−3826

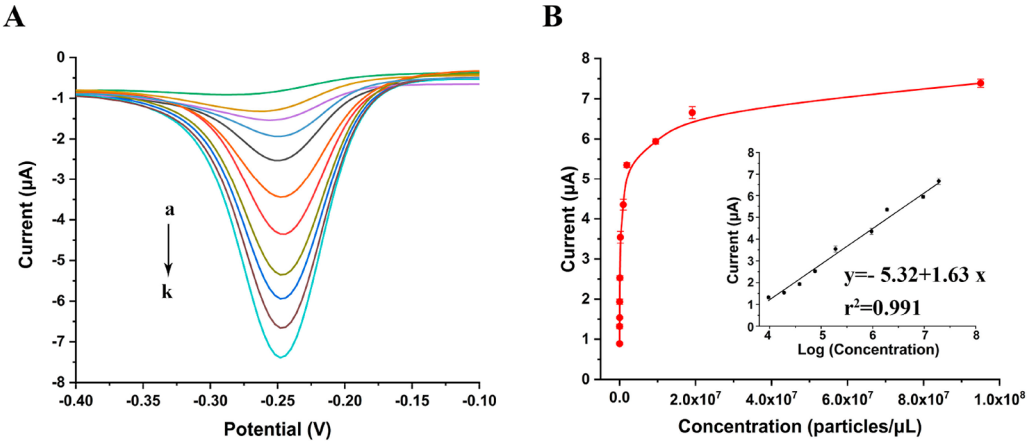

Figure 4. (A) SWV recorded with the different concentrations of exosomes, a–k (particles/μL): 0, 9.5×10^3, 1.9×10^4, 3.8×10^4, 7.6×10^4, 1.9×10^5, 9.5×10^5, 1.9×10^6, 9.5×10^6, 1.9×10^7, 9.5×10^7. (B) Relationship between the values of peak current and the concentrations. Inset is the linear range. Error bars represent the standard derivation of three independent experiments.

appear in the MB@UiO-66, which prove that MB is encapsulated in UiO-66-NH_2.[51] Moreover, the amount of MB in the MOF has been determined by UV/vis spectroscopy and the loading rate is 65.35% (SI Figure S9).[52]

Characterization of Exosomes. Exosomes pellets are isolated from the U87 GBM cells supernatant based on the differential centrifugation method. The physical characteristics are measured by NanoSight, revealing that the concentration is ~1.9×10^7 particles/μL with a size of about 80 nm (SI Figure S2A). Transmission electron microscope (TEM) image has also been performed to examine the morphology, showing a typical membrane-bound vesicle with the diameters consistent with the size of NanoSight (SI Figure S2B). These results corroborate with previously reported evidence, suggesting that the isolated exosomes can be used for the biosensor construction.

Feasibility Validation of the Biosensor. The electrochemical biosensor has been first investigated by electrochemical impedance spectroscopy (EIS) with $Fe(CN)_6^{3-/4-}$ redox couple. As shown in Figure 2A, the bare gold electrode exhibits similar to a straight line (curve a), implying little electron transfer resistance. However, after the electrode is modified step-by-step with peptide, exosomes, and MB@UiO-66, the diameter of semicircles increase gradually (curve b,d). As the diameter of the semicircle represents the electron transfer resistance at the electrode interface, it is clearly confirmed the process of electrode modification and the binding of exosomes with peptide, as well MB@UiO-66. Second, the square wave voltammograms (SWV) are measured in the Tris-HCl buffer to verify the feasibility and specificity of this biosensor. As shown in Figure 2B, only small current signals are observed when applying SWV scan to the bare electrode (curve a) or exosomes-free electrode (curve b), indicating that there is no electron communication at the electrode surface. While a significant peak can be detected in the present of exosomes under the same condition (curve c), which confirm the viability of this biosensor for detection of exosomes.

Optimization of Experimental Conditions. In order to achieve the best performance of the biosensor for exosomes detection, the effects of corresponding experimental conditions on the biosensor have been optimized by conducting the following experiments. First, the concentration and incubation time of peptide have been optimized, since they are the important consideration in the modification of electrode surface. The results demonstrate that the highest electrochemical signal can be detected by using 5 μM peptide after incubation for 16 h (SI Figures S3 and S4). The peptide-functionalized electrode is then used to capture exosomes and the optimized time is shown to be 2 h (SI Figure S5). Under the optimum conditions of the modification of electrode surface, we investigate the reaction time and the amounts of MB@UiO-66 by detecting 1.9×10^7 particles/μL exosomes using the biosensor. With the prolonging of incubation time of MB@UiO-66, the current intensity increases continuously and almost reaches a plateau at 30 min (Figure 3A,B). So, 30 min is chosen as the optimal incubation time. Then, the concentration of MB@UiO-66 is optimized by binding with exosomes or exosomes-free electrode for 30 min. The SWV results indicate that 0.5 mg/mL of MB@UiO-66 can provide high signal readout with low background (Figure 3C,D). Therefore, 0.5 mg/mL is chosen as the optimal concentration of MB@UiO-66 for the following experiments.

Performance of the Biosensor. Under the optimized experimental conditions, the fabricated biosensor has been employed for the quantitative analysis of GBMs-derived exosomes. SWV measurement is carried out and the results of exosomes analysis at different concentrations are displayed in Figure 4A. With the amounts of exosomes increasing, the electrochemical currents enhance gradually. A linear relationship can be established between the peak currents and the logarithm of exosomes concentrations ranging from 9.5×10^3 to 1.9×10^7 particles/μL, with a linear equation of $y = -5.32 + 1.36\ x$ (Figure 4B). It can be estimated that the 7.83×10^3 particles/μL is the lowest detected concentration, which equal to the sum of background signal and three standard deviations ($y = 0.892\ \mu A + 3 \times 0.045\ \mu A = 1.027\ \mu A$). Meanwhile, the limit of detection (LOD) of our proposed biosensor has been compared with other previous reports, indicating its high sensitivity and large linear range for exosomes detection (SI Table S1). The selectivity of this method is further demonstrated by detecting same numbers of exosomes derived from different cells (SI Figure S7). The reproducibility of electrochemical biosensor is conducted by detecting exosomes at the concentration of 9.5×10^5 particles/μL (SI Figure S8), and the value of the relative standard deviation is 2.34% (n =

https://dx.doi.org/10.1021/acs.analchem.9b05241
Anal. Chem. 2020, 92, 3819–3826

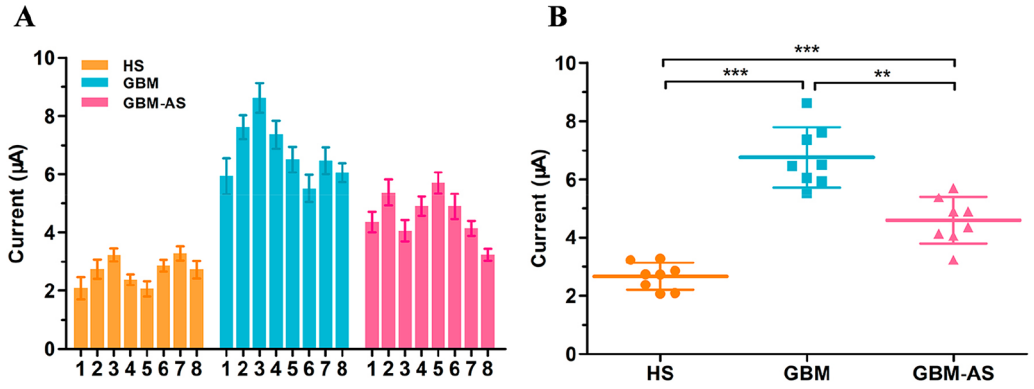

Figure 5. Clinical analyses of GBM-derived exosomes using this sensor. (A) The SWV currents and (B) scattered dot plots of exosomes obtained from serum samples of HS, GBM, and GBM-AS. The statistical significances of the observed difference are determined by *t* test, (***, $p < 0.0001$, **, $p < 0.001$). Error bars represent the standard deviation of three independent experiments.

6). Moreover, exosomes spiked in human serum are also challenged. As shown in SI Figure S6, under the same experimental conditions, the signal responses of exosomes diluted into serum are almost consistent with that in buffer, indicating that the biological matrix environment has little effect on the sensor. These results suggest that the biosensor can work well in the complex biological samples. Significantly, the GBM-derived exosomes in human serum can be detected by our sensor, as demonstrated in the following study.

Clinical Sample Analysis. To test the clinically diagnosis application of our biosensor, human serum are collected from 24 clinical samples of eight healthy individuals (HS), eight patients with GBM (GBM), and eight patients after surgery (GBM-AS). As shown in Figure 5A, current signals of exosomes from healthy serum are significantly lower than GBMs patients and postoperative, consistent with the published report that a higher expression of EGFR/EGFRvIII in GBM-derived exosomes than normal cells.[53] The statistical analysis of these results is also conducted and the scattered dot plots clearly show that there is a significant difference between the healthy group and GBM patients (Figure 5B). Notably, the measured SWV currents of exosomes in GBM-AS are less than those before surgery, indicating the capacity of our sensor for preand postsurgical monitoring of GBM patients. These results not only verify that the EGFR/EGFRvIII positive exosomes in serum can be used as biomarkers but also demonstrate the capacity of our sensor for early diagnosis, preand postsurgical monitoring of GBM patients.

CONCLUSIONS

In conclusion, we have successfully developed a label-free electrochemical biosensor for the detection of GBM-derived exosomes by using the Zr-based metal−organic frameworks. In the design of the biosensor, a peptide can selectively capture GBMs-derived exosomes through the highly expressed EGFR and EGFRvIII proteins. Meanwhile, based on the combination between Zr^{4+} and the exosomes surface, Zr-MOFs loaded with methylene blue may approach to the electrode surface to generate a high electrochemical signal. Therefore, the concentration of exosomes can be directly quantified without extra recognition and amplification elements, while the sensor can show very high selectivity and sensitivity. Moreover, this biosensor has been employed to analyze GBM-derived exosomes in human serum and distinguish GBM patients from healthy groups, which has demonstrated the feasibility for early diagnosis and monitoring in GBM therapy. Furthermore, the strategy of the design can be to detect other disease biomarkers by simply replacing the capture sequences, showing the great prospective values to fabricate other clinical sensing platform.

ASSOCIATED CONTENT

Supporting Information

The Supporting Information is available free of charge at https://pubs.acs.org/doi/10.1021/acs.analchem.9b05241.

Experimental sections; Fourier transform infrared spectroscopy of MOF; corresponding square wave voltammograms; comparison of exosomes diluted in PBS and serum; comparisons of this biosensor with previous methods (PDF)

AUTHOR INFORMATION

Corresponding Authors

Yongmei Yin − *Department of Oncology, The First Affiliated Hospital of Nanjing Medical University, Nanjing 210029, P. R. China;* orcid.org/0000-0002-2996-3631; Email: ymyin@njmu.edu.cn; Fax: +86 25 68136043

Genxi Li − *State Key Laboratory of Pharmaceutical Biotechnology, School of Life Sciences, Nanjing University, Nanjing 210023, P. R. China; Center for Molecular Recognition and Biosensing, School of Life Sciences, Shanghai University, Shanghai 200444, P. R. China;* orcid.org/0000-0001-9663-9914; Email: genxili@nju.edu.cn; Fax: +86 25 83592510

Authors

Zhaowei Sun − *State Key Laboratory of Pharmaceutical Biotechnology, School of Life Sciences, Nanjing University, Nanjing 210023, P. R. China*

Lei Wang − *State Key Laboratory of Pharmaceutical Biotechnology, School of Life Sciences, Nanjing University, Nanjing 210023, P. R. China*

Shuai Wu − *State Key Laboratory of Pharmaceutical Biotechnology, School of Life Sciences, Nanjing University, Nanjing 210023, P. R. China;* orcid.org/0000-0001-6422-1599

Yanhong Pan − *State Key Laboratory of Pharmaceutical Biotechnology, School of Life Sciences, Nanjing University, Nanjing 210023, P. R. China*

https://dx.doi.org/10.1021/acs.analchem.9b05241
Anal. Chem. 2020, 92, 3819−3826

Yu Dong − *Department of Neurosurgery, Nanjing Integrated Traditional Chinese and Western Medicine Hospital, Affiliated with Nanjing University of Chinese Medicine, Nanjing 210014, P. R. China*

Sha Zhu − *Department of Oncology, The Affiliated Wuxi No.2 People's Hospital of Nanjing Medical University, Wuxi 214000, P. R. China*

Jie Yang − *State Key Laboratory of Pharmaceutical Biotechnology, School of Life Sciences, Nanjing University, Nanjing 210023, P. R. China*

Complete contact information is available at: https://pubs.acs.org/10.1021/acs.analchem.9b05241

Notes

The authors declare no competing financial interest.

■ ACKNOWLEDGMENTS

This work was supported by the National Natural Science Foundation of China (Grant No. 81772593).

■ REFERENCES

(1) Louis, D. N.; Perry, A.; Reifenberger, G.; von Deimling, A.; Figarella-Branger, D.; Cavenee, W. K.; Ohgaki, H.; Wiestler, O. D.; Kleihues, P.; Ellison, D. W. *Acta Neuropathol.* **2016**, *131* (6), 803−820.

(2) Choi, B. D.; Archer, G. E.; Mitchell, D. A.; Heimberger, A. B.; McLendon, R. E.; Bigner, D. D.; Sampson, J. H. *Brain Pathol.* **2009**, *19* (4), 713−723.

(3) Reifenberger, G.; Wirsching, H. G.; Knobbe-Thomsen, C. B.; Weller, M. *Nat. Rev. Clin. Oncol.* **2017**, *14* (7), 434−452.

(4) Chinot, O. L.; Wick, W.; Mason, W.; Henriksson, R.; Saran, F.; Nishikawa, R.; Carpentier, A. F.; Hoang-Xuan, K.; Kavan, P.; Cernea, D.; Brandes, A. A.; Hilton, M.; Abrey, L.; Cloughesy, T. *N. Engl. J. Med.* **2014**, *370* (8), 709−722.

(5) Stupp, R.; Taillibert, S.; Kanner, A. A.; Kesari, S.; Steinberg, D. M.; Toms, S. A.; Taylor, L. P.; Lieberman, F.; Silvani, A.; Fink, K. L.; Barnett, G. H.; Zhu, J.-J.; Henson, J. W.; Engelhard, H. H.; Chen, T. C.; Tran, D. D.; Sroubek, J.; Tran, N. D.; Hottinger, A. F.; Landolfi, J.; Desai, R.; Caroli, M.; Kew, Y.; Honnorat, J.; Idbaih, A.; Kirson, E. D.; Weinberg, U.; Palti, Y.; Hegi, M. E.; Ram, Z. *JAMA* **2015**, *314* (23), 2535−2543.

(6) Stupp, R.; Mason, W. P.; van den Bent, M. J.; Weller, M.; Fisher, B.; Taphoorn, M. J.; Belanger, K.; Brandes, A. A.; Marosi, C.; Bogdahn, U.; Curschmann, J.; Janzer, R. C.; Ludwin, S. K.; Gorlia, T.; Allgeier, A.; Lacombe, D.; Cairncross, J. G.; Eisenhauer, E.; Mirimanoff, R. O. *N. Engl. J. Med.* **2005**, *352* (10), 987−996.

(7) Hishii, M.; Matsumoto, T.; Arai, H. *Asian J. Neurosurg* **2019**, *14* (2), 589−592.

(8) Wang, F.; Zheng, Z.; Guan, J.; Qi, D.; Zhou, S.; Shen, X.; Wenkert, D.; Kirmani, B.; Solouki, T.; Fonkem, E.; Wong, E. T.; Huang, J. H.; Wu, E. *EBioMedicine* **2018**, *37*, 68−77.

(9) Ryken, T. C.; Aygun, N.; Morris, J.; Schweizer, M.; Nair, R.; Spracklen, C.; Kalkanis, S. N.; Olson, J. J. *J. Neuro-Oncol.* **2014**, *118* (3), 435−460.

(10) Utsuki, S.; Oka, H.; Miyajima, Y.; Kijima, C.; Yasui, Y.; Fujii, K. *Int. J. Clin. Med.* **2012**, *03* (06), 439−445.

(11) Ideguchi, M.; Kajiwara, K.; Goto, H.; Sugimoto, K.; Nomura, S.; Ikeda, E.; Suzuki, M. *J. Neuro-Oncol.* **2015**, *123* (2), 289−297.

(12) Drean, A.; Goldwirt, L.; Verreault, M.; Canney, M.; Schmitt, C.; Guehennec, J.; Delattre, J. Y.; Carpentier, A.; Idbaih, A. *Expert Rev. Neurother.* **2016**, *16* (11), 1285−1300.

(13) Anastasiadou, E.; Slack, F. J. *Science* **2014**, *346* (6216), 1459.

(14) Kowal, J.; Tkach, M.; Thery, C. *Curr. Opin. Cell Biol.* **2014**, *29*, 116−125.

(15) Valadi, H.; Ekström, K.; Bossios, A.; Sjöstrand, M.; Lee, J. J.; Lötvall, J. O. *Nat. Cell Biol.* **2007**, *9* (6), 654−659.

(16) Thoms, M.; Thomson, E.; Bassler, J.; Gnadig, M.; Griesel, S.; Hurt, E. *Cell* **2015**, *162* (5), 1029−1038.

(17) Alvarez-Erviti, L.; Seow, Y.; Yin, H.; Betts, C.; Lakhal, S.; Wood, M. J. *Nat. Biotechnol.* **2011**, *29* (4), 341−345.

(18) Kalluri, R. *J. Clin. Invest.* **2016**, *126* (4), 1208−1215.

(19) Saadatpour, L.; Fadaee, E.; Fadaei, S.; Nassiri Mansour, R.; Mohammadi, M.; Mousavi, S. M.; Goodarzi, M.; Verdi, J.; Mirzaei, H. *Cancer Gene Ther.* **2016**, *23* (12), 415−418.

(20) Xu, H.; Zhang, K.; Zong, H.; Shang, M.; Li, K.; He, X. *Journal of B.U.ON.: official journal of the Balkan Union of Oncology* **2016**, *21* (6), 1368−1373.

(21) Figueroa, J. M.; Skog, J.; Akers, J.; Li, H.; Komotar, R.; Jensen, R.; Ringel, F.; Yang, I.; Kalkanis, S.; Thompson, R.; LoGuidice, L.; Berghoff, E.; Parsa, A.; Liau, L.; Curry, W.; Cahill, D.; Bettegowda, C.; Lang, F. F.; Chiocca, E. A.; Henson, J.; Kim, R.; Breakefield, X.; Chen, C.; Messer, K.; Hochberg, F.; Carter, B. S. *Neuro Oncol* **2017**, *19* (11), 1494−1502.

(22) Zadeh, G.; Bhat, K. P.; Aldape, K. *Cancer Cell* **2013**, *24* (4), 403−4.

(23) Verhaak, R. G.; Hoadley, K. A.; Purdom, E.; Wang, V.; Qi, Y.; Wilkerson, M. D.; Miller, C. R.; Ding, L.; Golub, T.; Mesirov, J. P.; Alexe, G.; Lawrence, M.; O'Kelly, M.; Tamayo, P.; Weir, B. A.; Gabriel, S.; Winckler, W.; Gupta, S.; Jakkula, L.; Feiler, H. S.; Hodgson, J. G.; James, C. D.; Sarkaria, J. N.; Brennan, C.; Kahn, A.; Spellman, P. T.; Wilson, R. K.; Speed, T. P.; Gray, J. W.; Meyerson, M.; Getz, G.; Perou, C. M.; Hayes, D. N. *Cancer Cell* **2010**, *17* (1), 98−110.

(24) Brennan, C. W.; Verhaak, R. G.; McKenna, A.; Campos, B.; Noushmehr, H.; Salama, S. R.; Zheng, S.; Chakravarty, D.; Sanborn, J. Z.; Berman, S. H.; Beroukhim, R.; Bernard, B.; Wu, C. J.; Genovese, G.; Shmulevich, I.; Barnholtz-Sloan, J.; Zou, L.; Vegesna, R.; Shukla, S. A.; Ciriello, G.; Yung, W. K.; Zhang, W.; Sougnez, C.; Mikkelsen, T.; Aldape, K.; Bigner, D. D.; Van Meir, E. G.; Prados, M.; Sloan, A.; Black, K. L.; Eschbacher, J.; Finocchiaro, G.; Friedman, W.; Andrews, D. W.; Guha, A.; Iacocca, M.; O'Neill, B. P.; Foltz, G.; Myers, J.; Weisenberger, D. J.; Penny, R.; Kucherlapati, R.; Perou, C. M.; Hayes, D. N.; Gibbs, R.; Marra, M.; Mills, G. B.; Lander, E.; Spellman, P.; Wilson, R.; Sander, C.; Weinstein, J.; Meyerson, M.; Gabriel, S.; Laird, P. W.; Haussler, D.; Getz, G.; Chin, L.; et al. *Cell* **2013**, *155* (2), 462−477.

(25) Mao, J.; Ran, D.; Xie, C.; Shen, Q.; Wang, S.; Lu, W. *ACS Appl. Mater. Interfaces* **2017**, *9* (29), 24462−24475.

(26) Dragovic, R. A.; Gardiner, C.; Brooks, A. S.; Tannetta, D. S.; Ferguson, D. J.; Hole, P.; Carr, B.; Redman, C. W.; Harris, A. L.; Dobson, P. J.; Harrison, P.; Sargent, I. L. *Nanomedicine* **2011**, *7* (6), 780−788.

(27) Moon, P. G.; Lee, J. E.; Cho, Y. E.; Lee, S. J.; Jung, J. H.; Chae, Y. S.; Bae, H. I.; Kim, Y. B.; Kim, I. S.; Park, H. Y.; Baek, M. C. *Clin. Cancer Res.* **2016**, *22* (7), 1757−1766.

(28) Nolte-'t Hoen, E. N.; van der Vlist, E. J.; Aalberts, M.; Mertens, H. C.; Bosch, B. J.; Bartelink, W.; Mastrobattista, E.; van Gaal, E. V.; Stoorvogel, W.; Arkesteijn, G. J.; Wauben, M. H. *Nanomedicine* **2012**, *8* (5), 712−720.

(29) Im, H.; Shao, H.; Park, Y. I.; Peterson, V. M.; Castro, C. M.; Weissleder, R.; Lee, H. *Nat. Biotechnol.* **2014**, *32* (5), 490−495.

(30) Stremersch, S.; Marro, M.; Pinchasik, B. E.; Baatsen, P.; Hendrix, A.; De Smedt, S. C.; Loza-Alvarez, P.; Skirtach, A. G.; Raemdonck, K.; Braeckmans, K. *Small* **2016**, *12* (24), 3292−3301.

(31) Wang, L.; Yang, Y.; Liu, Y.; Ning, L.; Xiang, Y.; Li, G. *Chem. Commun.* **2019**, *55* (18), 2708−2711.

(32) He, F.; Wang, J.; Yin, B. C.; Ye, B. C. *Anal. Chem.* **2018**, *90* (13), 8072−8079.

(33) Doldan, X.; Fagundez, P.; Cayota, A.; Laiz, J.; Tosar, J. P. *Anal. Chem.* **2016**, *88* (21), 10466−10473.

(34) Boriachek, K.; Masud, M. K.; Palma, C.; Phan, H. P.; Yamauchi, Y.; Hossain, M. S. A.; Nguyen, N. T.; Salomon, C.; Shiddiky, M. J. A. *Anal. Chem.* **2019**, *91* (6), 3827−3834.

(35) Kreno, L. E.; Leong, K.; Farha, O. K.; Allendorf, M.; Van Duyne, R. P.; Hupp, J. T. *Chem. Rev.* **2012**, *112* (2), 1105−1125.

(36) Zhang, S. Y.; Shi, W.; Cheng, P.; Zaworotko, M. J. *J. Am. Chem. Soc.* **2015**, *137* (38), 122031220−6.
(37) Wang, J.-H.; Li, M.; Li, D. *Chemical Science* **2013**, *4* (4), 1793.
(38) Sun, Z.; Wu, S.; Ma, J.; Shi, H.; Wang, L.; Sheng, A.; Yin, T.; Sun, L.; Li, G. *ACS Appl. Mater. Interfaces* **2019**, *11* (40), 36316−36323.
(39) Wang, Z.; Yan, Z.; Wang, F.; Cai, J.; Guo, L.; Su, J.; Liu, Y. *Biosens. Bioelectron.* **2017**, *97*, 107−114.
(40) Wu, S.; Li, C.; Shi, H.; Huang, Y.; Li, G. *Anal. Chem.* **2018**, *90* (16), 9929−9935.
(41) Heck, J. G.; Napp, J.; Simonato, S.; Mollmer, J.; Lange, M.; Reichardt, H. M.; Staudt, R.; Alves, F.; Feldmann, C. *J. Am. Chem. Soc.* **2015**, *137* (23), 7329−7336.
(42) Zhang, G. Y.; Zhuang, Y. H.; Shan, D.; Su, G. F.; Cosnier, S.; Zhang, X. J. *Anal. Chem.* **2016**, *88* (22), 11207−11212.
(43) Yan, Z.; Wang, F.; Deng, P.; Wang, Y.; Cai, K.; Chen, Y.; Wang, Z.; Liu, Y. *Biosens. Bioelectron.* **2018**, *109*, 132−138.
(44) Zhu, X.; Li, B.; Yang, J.; Li, Y.; Zhao, W.; Shi, J.; Gu, J. *ACS Appl. Mater. Interfaces* **2015**, *7* (1), 223−231.
(45) Denholt, C. L.; Binderup, T.; Stockhausen, M. T.; Poulsen, H. S.; Spang-Thomsen, M.; Hansen, P. R.; Gillings, N.; Kjaer, A. *Nucl. Med. Biol.* **2011**, *38* (4), 509−15.
(46) Li, H.; Huang, Y.; Yu, Y.; Wang, Y.; Li, G. *Biosens. Bioelectron.* **2016**, *80*, 560−565.
(47) Li, H.; Cao, Y.; Wu, X.; Ye, Z.; Li, G. *Talanta* **2012**, *93*, 358−63.
(48) Li, C.; Hu, X.; Lu, J.; Mao, X.; Xiang, Y.; Shu, Y.; Li, G. *Chem. Sci.* **2018**, *9* (4), 979−984.
(49) Gu, J. Y.; Lu, X. J.; Ju, H. X. *Electroanalysis* **2002**, *14* (13), 949−954.
(50) Li, H.; Huang, Y.; Zhang, B.; Pan, X.; Zhu, X.; Li, G. *Anal. Chem.* **2014**, *86* (24), 12138−42.
(51) Chang, J.; Wang, X.; Wang, J.; Li, H.; Li, F. *Anal. Chem.* **2019**, *91* (5), 3604−3610.
(52) Zheng, H.; Zhang, Y.; Liu, L.; Wan, W.; Guo, P.; Nystrom, A. M.; Zou, X. *J. Am. Chem. Soc.* **2016**, *138* (3), 962−8.
(53) Choi, D.; Montermini, L.; Kim, D. K.; Meehan, B.; Roth, F. P.; Rak, J. *Mol. Cell. Proteomics* **2018**, *17* (10), 1948−1964.

https://dx.doi.org/10.1021/acs.analchem.9b05241
Anal. Chem. 2020, 92, 3819−3826